Original Article

Institution of MECHANICAL ENGINEERS

Journal of RAIL AND RAPID TRANSIT

Proc IMechE Part F:
J Rail and Rapid Transit
0(0) 1–12

DOI: 10.1177/0954409712458496
pif.sagepub.com

SAGE

Assessing the effects of track input on the response of insulated rail joints using field experiments

Hossein Askarinejad[1,2], Manicka Dhanasekar[2,3] and Colin Cole[1,2]

Abstract

Manufacturers of insulated rail joints (IRJs) have to follow the quality assurance regime stipulated in the national design standards; unfortunately, IRJs still exhibit a very low and highly variable service life. It is widely believed that the service life of IRJs is affected by the track input under the passage of loaded wheels; however, there is a paucity of literature with regard to the actual mechanical behaviour of IRJs in the track. An extensive field test was, therefore, conducted on an in-service heavy haul corridor in Australia with the specific aim of understanding the effect of the track input on the response of the IRJs. Data on the wheel–rail force, rail/joint-bar strain, sleeper acceleration and ballast pressure signatures in the time domain were determined from the experiment. This data was subsequently systematically analysed to compare the relative structural merits of two IRJs resting on different sleeper spaces and a reference continuous rail subjected to similar real-life coal traffic loading.

Keywords

Insulated rail joint, field testing, wheel–rail force, rail strains, sleeper acceleration, sleeper–ballast pressure

Date received: 30 January 2012; accepted: 12 July 2012

Introduction

In a typical insulated rail joint (IRJ), the ends of the adjoining rails are connected using two joint bars (fishplates) on both sides of the rail web, then the joint bars are electrically insulated from the rail and the gap in the joint is filled with an insulating material, known as end post. As a result of the continuing demand for resources, the throughput on coal rail lines is on the rise in Australia; the need for IRJs as the integral component of the automatic block signalling system is also, therefore, on the increase.

It is widely believed that the low bending stiffness of joint bars compared with that for the rail section results in the generation of impact forces and high vertical deflection under the passage of wheels, which subsequently leads to different deterioration modes of the IRJs such as rail head damage, bolt looseness, joint-bar fracture and ballast deterioration (Figure 1).

The performance of IRJs has become a significant economic problem for the rail industry as evidenced by the increased number of publications in recent times.[1-10] The majority of these publications describe analytical and numerical modelling of the IRJs, with only a limited amount of experimental work being presented. Some studies have focussed on methods to improve the material or geometry properties (structural shape) of the IRJ components.[2-4] These modifications, while being expensive, have not made any considerable improvement in the IRJ service life in heavy haul lines. For instance, Plaut et al.[2] discussed the tapered insulated joint. They reported that in comparison with a conventional IRJ, the tapered joint exhibited smaller values of bending stress and shear stress in the joint and the adhesive, respectively, comparing with traditional joints. However, it can experience higher metal flow at the surface and some additional torsional displacement due to its asymmetrical section within the tapered length. Moreover, the use of a thick web rail in the tapered joint obviously adds cost because of the additional steel and it has to transition back to the traditional rail at the end.[2]

[1]Centre for Railway Engineering, Central Queensland University, Australia
[2]CRC for Rail Innovations, Australia
[3]School of Civil Engineering and Built Environment, Queensland University of Technology, Australia

Corresponding author:
Manicka Dhanasekar, School of Civil Engineering and Built Environment, S-714, GP Campus, Queensland University of Technology, Brisbane, QLD4000, Australia.
Email: m.dhanasekar@qut.edu.au

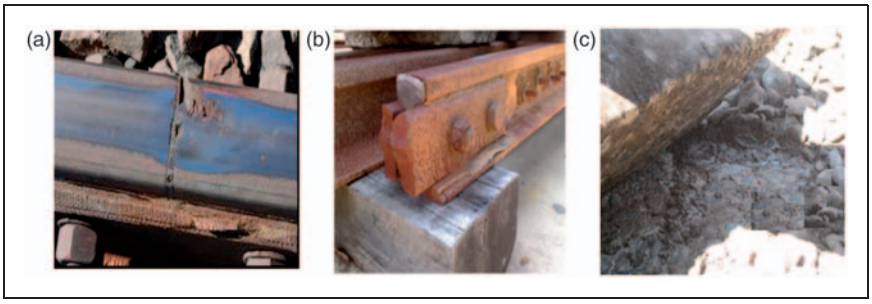

Figure 1. IRJ deterioration: (a) rail head damage; (b) broken joint bar; and (c) ballast deterioration beneath sleeper adjacent to IRJ.

Dhanasekar and Bayissa[4] presented the results of a field test that was performed to compare the performance of IRJs with square-cut and inclined-cut joints based on the strain signatures near the rail head adjacent to the gap measured under traffic loading. They reported that although the vertical strains near the rail head of the inclined IRJ were smaller than those of the square IRJ, the inclined IRJ experienced higher shear strains near the throat of the rails.

On the other hand, recently it has been reported that even IRJs with similar structural and material properties and under similar traffic conditions show variable performance in different locations. A research hypothesis was, therefore, put forward that the track condition or the properties of the support beneath the IRJs significantly affect their behaviour. In other words, local modification of track/support condition beneath the IRJ may provide an efficient and economical way to significantly improve the service life of these factory assembled components in track. A review of the literature indicated that there exists a gap in knowledge on the benefits or otherwise of local modification of the support system beneath IRJs. Some work on the effect of support condition on IRJ performance has been carried out by Suzuki et al.[5] and Akhtar et al.[6] Suzuki et al.[5] performed field measurements on the wheel–rail force at rail joints and examined the data for the effects of dynamic loads in terms of a vertical dip around the joint gap. They used the field measurements to validate a vehicle–track dynamic model which was employed to study the effect of gap length in the joint and vertical dip on the wheel–rail vertical force. They concluded that the presence of a vertical dip at the IRJ as a result of a deteriorated foundation or deformed rail head had more influence on the dynamic loads than increasing the joint gap from 6 to 11 mm. Akhtar et al.[6] reported the results of tests on different designs of IRJs, with increased length of joint bar, different joint gap shapes and foundation conditions. They reported that there is a strong correlation between foundation condition and IRJ service life. They considered a poor foundation as one that had muddy ballast or rail fastener and sleeper problems.

In this paper, an extensive experimental work is reported in which two IRJs and a continuous rail section were instrumented with a significant number of sensors and monitored in service under coal train traffic loading. Understanding the behaviour of the IRJs and the associated track components under real-life traffic loading is essential if appropriate methods are to be developed to handle, install and maintain the IRJs in order to extend their service life. The main objectives of this research include:

- examining the track responses at IRJs and that of the continuously welded rail;
- evaluating the effect of the support system on the behaviour of the IRJs.

An experiment on this scale on the behaviour of IRJs has not been previously carried out and the results provide new information hitherto unavailable in the literature; wheel–rail force, rail/joint-bar strain, sleeper acceleration and ballast pressure signatures in the time domain under real-life traffic loading are used as the primary illustration of the behaviour of IRJs in track.

Theoretical considerations

An IRJ is considered to be a section with an abrupt vertical stiffness reduction in the track. The abrupt stiffness discontinuity can vary in different locations with different track properties. The severity of this stiffness discontinuity can also change over time due to track deterioration (support beneath the immediate vicinity of the gaps), which subsequently can aggravate the loads and responses.

Therefore, it is assumed that an improvement in the support system beneath the IRJ should partly offset the stiffness reduction and also reduce the rate at which track deterioration occurs. The practice of spacing the sleepers at a rail joint closer together can be an easy way to locally stiffen the track beneath a joint. With direct positioning of one sleeper beneath the joint as well as a non-symmetric arrangement of sleepers with respect to the joint gap, an excess of pressure beneath the sleeper can be found, giving rise to ballast deterioration and subsequent overloading of the joint. Therefore, it is assumed that the symmetric arrangement of a number of closely spaced sleepers around a joint gap will result in higher

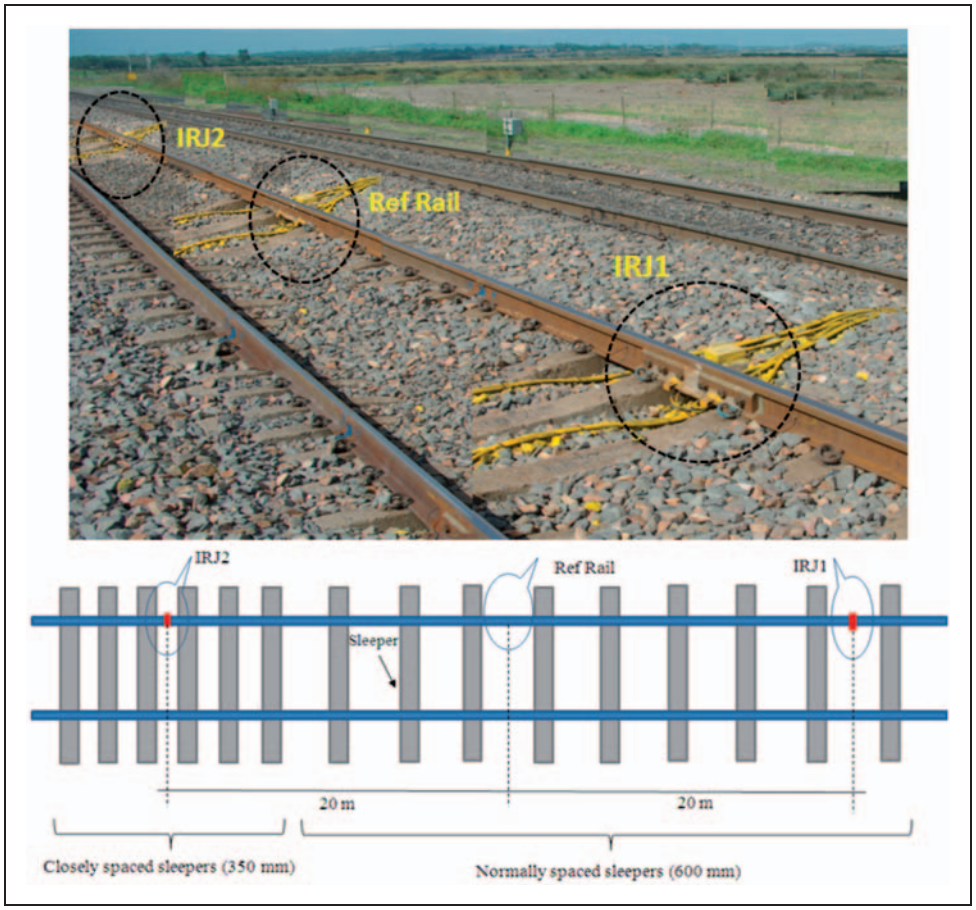

Figure 2. Field test setup.

stiffness levels, a better distribution of sleeper pressure and less track deterioration over time. This subsequently will lower the responses of the IRJs which will generally prolong the life of the IRJs. Two IRJs, one resting on a normal support arrangement and the other on closely spaced sleepers were fully instrumented and monitored in the performed field test. In addition, a continuous rail section (reference rail) was also instrumented with a sensor arrangement similar to the one for the two IRJs. The reference rail provided a measure of the wheel load that was benchmarked with weighbridge data. Furthermore, a comparison of the wheel load, rail strain, sleeper acceleration and ballast pressure captured by the reference rail and the IRJs allows the quantification of the load and responses in the vicinity of the gap of the IRJs. The results of this comparison can be used to potentially improve the handling, placement and maintenance of IRJs.

Field test setup

A view of test setup is presented in Figure 2. The test site was subjected to a fairly uniform traffic condition in terms of types of trains, speed and axle loads. The line is uni-directional servicing only loaded coal trains with high axle loads. The IRJs and reference rail were fully instrumented. The sensor cables were taken through conduits to the access road and were terminated with plugs in a trackside terminal box. The total length of the instrumented test site was 40 m divided into three sections including the IRJ1 and reference rail with regular support condition (600 mm sleeper spacing), and IRJ2 with modified support condition (six sleepers with the reduced spacing of 350 mm). The track substructure was fairly uniform along the length of the test site. The overall track bed thickness was 450 mm including a ballast layer of 300 mm and a capping layer of 150 mm. The particle size, graduation and other properties of the ballast material at the test site were in accordance with the technical specification TS 3402, Rail Infrastructure Corporation of New South Wales.[11] The two IRJs were produced in a factory using thermosetting glueing process of insulating materials within a furnace following the stringent quality processes conforming to AS1085.12.[12]

The instrumentation

The reference rail was strain gauged in the laboratory. The rail web of the IRJs (between rail and joint bar) was strain gauged within the factory setup involving the furnace process and the joint bars were strain gauged in the laboratory. The location of strain

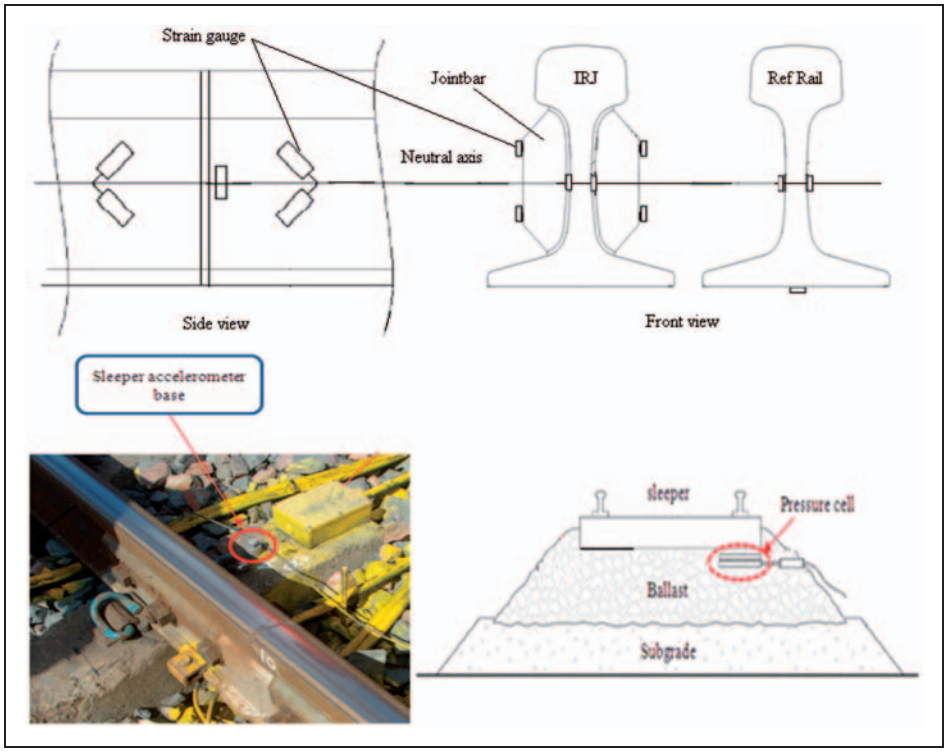

Figure 3. Location of sensors.

gauges on the IRJs and the reference rail is presented in Figure 3. Longitudinal strain gauges were used to measure the rail bending strains generated under the wheel load; in the reference rail, the longitudinal strain gauge was installed at the bottom of the rail and in the IRJs, the longitudinal strain gauges were installed on the top and bottom of the joint bars since at the joint gap the whole bending moment is carried by the joint bars. To capture the maximum bending strains on the joint bars, the strain gauges were mounted at the highest practical distance to the neutral axis on both sides. The strain gauges on the rail web were bridged to form a load detector to measure the wheel–rail force at IRJs and the reference rail.[13]

A combination of multiple-element shear strain gauges and single vertical strain gauges installed on the rail web were used to estimate the values of the wheel–rail vertical force on the IRJs and the reference rail; multiple-element shear strain gauges were mounted on the neutral axis of the rail web for this purpose. These strain gauges were wired into a full bridge circuit and calibrated to determine the vertical wheel–rail contact force over the joint. The shear bridge output is a function of the difference between the two shear forces induced in the rail cross-sections. Eight gauges were attached to the rail web at the level of the neutral axis, keeping the strain gauge gridlines at 45° to the rail axis and were then wired into a full bridge circuit. Considering that the only vertical load applied to the rail between the two instrumented sections was the moving wheel, the shear bridge output voltage will be constant during wheel passage producing a trapezoidal-shaped signal. Therefore, as the wheel passes over the instrumented zone any load variation introduced by the wheel or rail irregularities will influence the output signal shape showing the value of the dynamic impact within the instrumented section.[13]

The strain gauge-based wheel load detector has been previously used in the literature to measure vertical wheel–rail forces in particular the wheel–rail impact generated due to wheel flats.[14-16] However, due to the existing complexities in the geometry of rail joint assemblies and difficulties in positioning and mounting the strain gauges at rail joints, this technique appears to not to have been used to detect the wheel–rail forces generated at rail joints, as revealed by the literature. In this research, a strain gauge-based wheel load detector, for the first time, was used to measure the wheel–rail contact force at an IRJ in a heavy haul rail line. The theoretical background and the procedure for development, testing and calibration of the shear bridge wheel load indicator were discussed in Askarinejad and Dhanasekar[13].

The IRJs and the reference rail were transferred to the test site, installed in the track and instrumented with accelerometers and pressure cells. Accelerometers were mounted on top of the sleepers adjacent to the IRJs and the reference rail. Mounting bases were designed to allow adhesive mounting of the accelerometer to the sleeper (Figure 3). The accelerometers were connected to the bases only at the time of data recording and removed at the end of the day. The accelerometers were PCB sensors with a

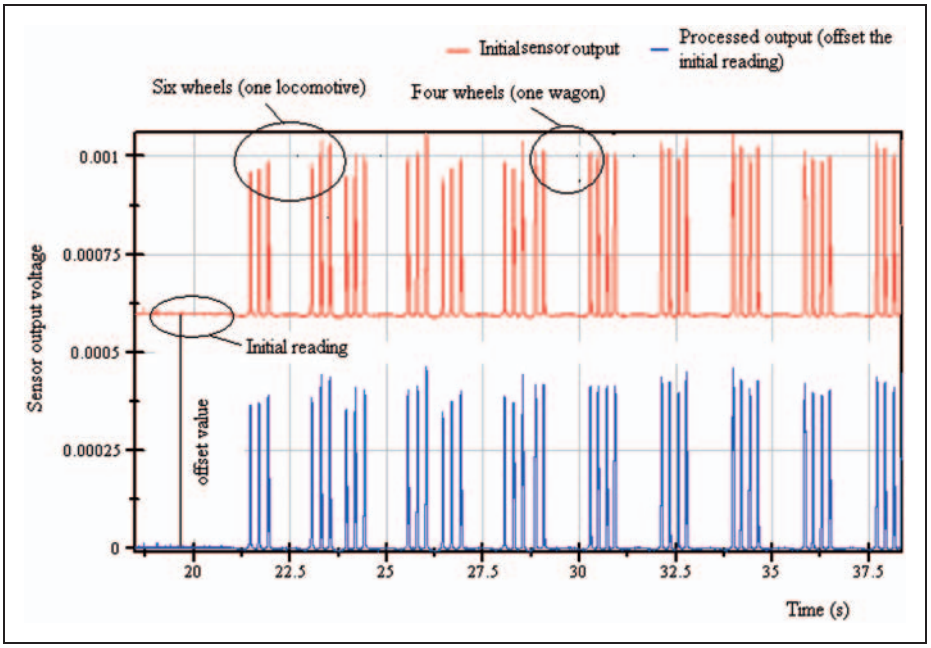

Figure 4. Offsetting the sensor's initial reading in the data post-processing.

frequency range of between 0.5 and 3000 Hz; similar ones were used by Chebli et al.[17] for in situ track measurements.

Hydraulic-type earth pressure cells capable of measuring dynamic pressures were selected for this experiment. The pressure cells were placed in the ballast directly below the sleeper to measure the sleeper–ballast pressure adjacent to the IRJ and the reference rail. In this type of pressure cell, two flat plates are welded together at their periphery and are separated by a small gap that is filled with a hydraulic fluid. The applied load squeezes the two plates together thus building up a pressure in the fluid. The accuracy and measurement range of this pressure cell model was suitable to capture the maximum expected sleeper–ballast contact pressure generated under a coal train. A similar type of pressure cell was used by Indraratna et al.[18] to assess pressure levels in track substructures. An image of the pressure cell and its location beneath the sleeper is presented in Figure 3.

Data analysis

A portable data acquisition system was connected to the plugs in the trackside terminal box at the time of data logging. The data acquisition plan was programmed in LABVIEW with a sampling frequency of 10,000 samples/s. This sampling frequency ensured that all of the high-frequency dynamic impacts and the corresponding structural responses were recorded during the measurement. With this sampling frequency, a large amount of data was generated for each channel requiring a suitable and efficient method to sort through the data and extract the peak values and localized time histories for further examination.

Data analyses were conducted using the DIADEM commercial data analysis software. In the first step, the recorded signals were processed based on the initial output signals when there was no train on the test site. These measurements generated an initial value when there was no load on the rail; the measured value being due to small differences in the resistance of the strain gauges or due to the effect of temperature. Figure 4 shows an example of the time history of the output voltage from the shear strain gauge-bridge on the reference rail. The initial reading (before arrival of a train) and the contribution of each passing wheel is clearly observed. The initial readings were offset in the data post-processing so the sensor outputs purely represent the structural response due to the passing train.

Furthermore, the bending strains measured from both sides of the rail web and joint bars (gauge and field sides) were averaged to eliminate the effect of wheel eccentricity; only the averaged strain data were used in the analysis reported in this paper. The peak signals from each sensor were extracted and analysed. Prior to extraction of the peak signals, the recorded data were filtered using a low-pass filter to remove the high-frequency noise signals. An ideal low-pass filter removes the signal contents at frequencies higher than the cut-off frequency and does not affect the signals at frequencies lower than the cut-off frequency. The filtering algorithm was selected based on the expected frequency content of the required sensor output and also based on the characteristics of the data. For each sensor the filtered and unfiltered signals were plotted and compared in order to examine the accuracy and suitability of the used filtering algorithm. Figure 5 shows a typical strain and acceleration signal before and after filtering.

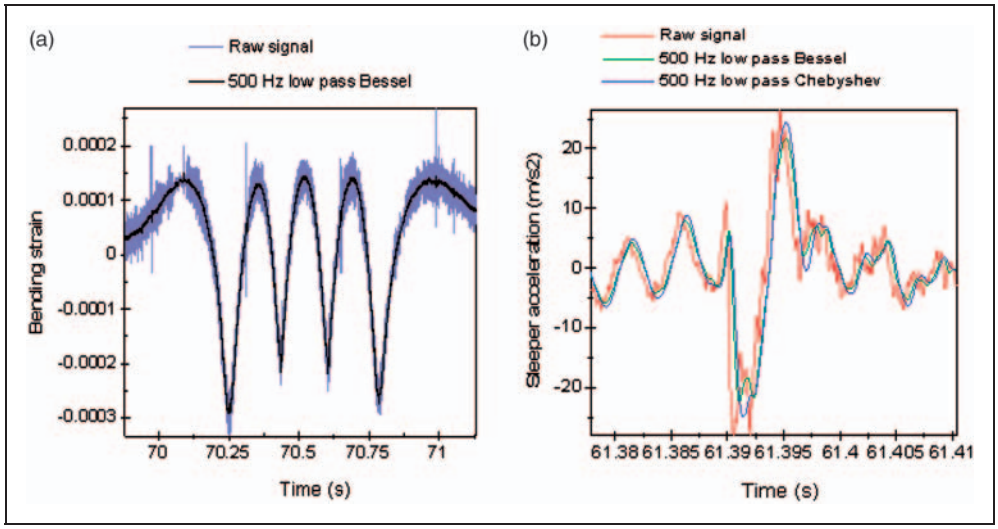

Figure 5. Low-pass filtering of the signals to remove the environmental noise (a) a typical strain signal and (b) a typical acceleration signal.

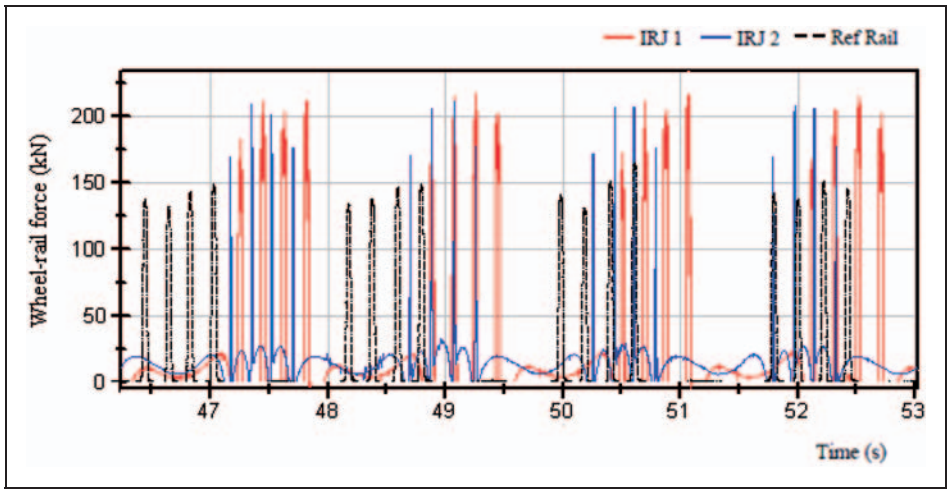

Figure 6. Time histories of wheel–rail force for a 7 s train passage.

Results

Wheel–rail vertical force

Typical time histories of the wheel–rail force values for an approximately 7 s passage of wheels across IRJ1, IRJ2 and the reference rail are presented in Figure 6. The peak values of the measured wheel–rail force are plotted in Figure 7. In this figure, the horizontal axis is 'wheel number' each one representing a wheel which has passed over the instrumented zone and the vertical axis presents the ratio of peak wheel–rail force (P) to the average value of the peak wheel–rail force on the reference rail (P_0). In this figure the data measured under 100 wagon wheels is presented and the locomotive wheels are not included. It can be seen that for the track condition and train speed considered in this test, the peak wheel–rail force

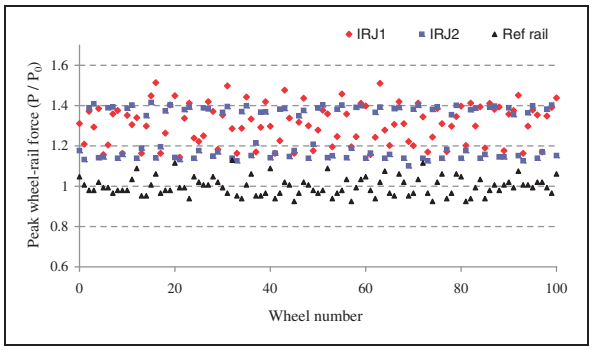

Figure 7. Peak wheel–rail force measured on the IRJs and the reference rail.

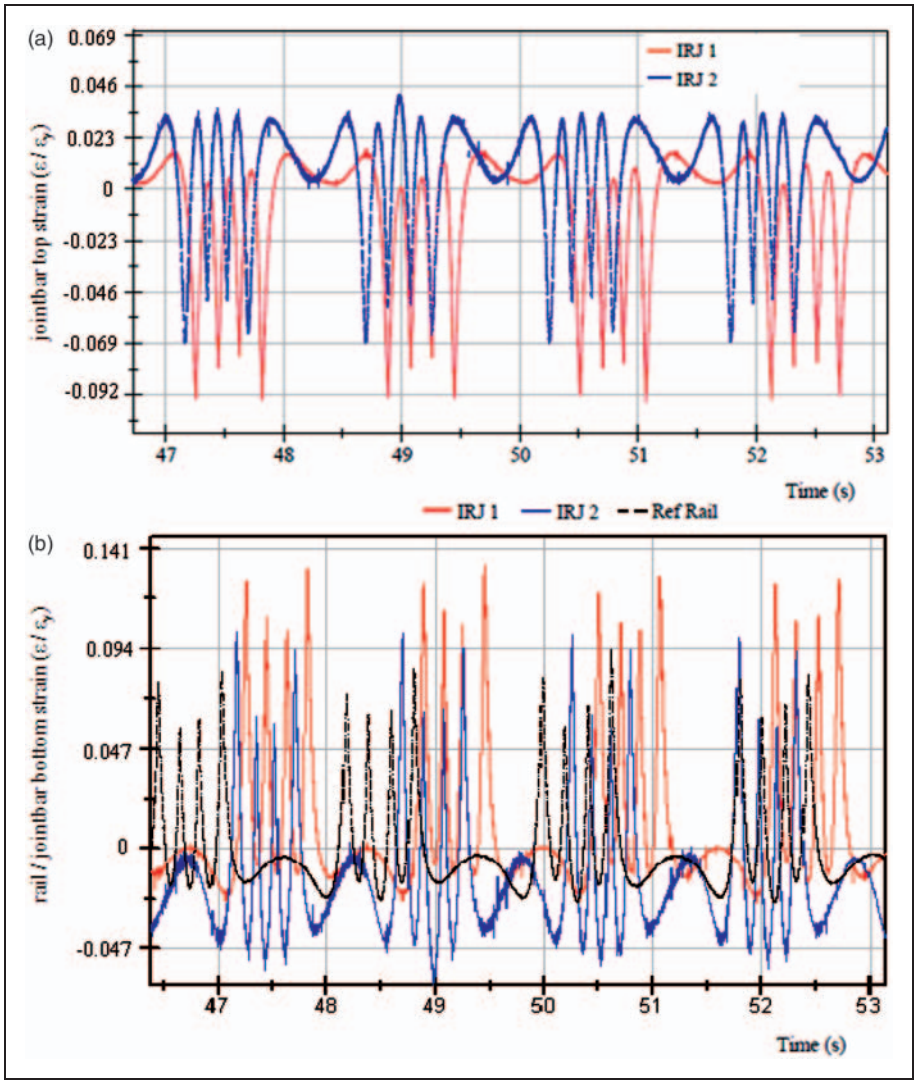

Figure 8. Time histories of bending strain for a 7 s train passage (a) joint bar top and (b) rail foot and joint bar bottom.

at the IRJ is on average 32% higher than that of the reference rail. The data recorded on the reference rail provides a measure of the wheel loads and the wheel–rail forces recorded on the IRJs demonstrate the increase in wheel–rail force (dynamic impact) due to the rail surface irregularity at the joint gap of the IRJ.

The wheel–rail impact force at the IRJ can increase for trains with higher speeds and also over time due to deterioration of the track geometry around the IRJ (assuming no change in loaded wagon mass, wheel roundness and suspension damping characteristics). The average peak wheel–rail impact at IRJ1 and IRJ2 do not show a considerable difference.

Rail/joint-bar bending strains

Typical averaged strain values from the gauge and field side of the joint bars for an approximately 7 s passage of wheels across IRJ1, IRJ2 and the reference rail are presented in Figure 8. For the IRJs, the measured strains at the top and bottom of the joint bar under the wheel passage are shown. The peak values of the bending strains extracted from the data are shown in Figure 9. In Figures 8 and 9, the vertical axis presents the ratio of the measured strain (ε) to the yield strain of rail steel (ε_y).

From Figure 9 it can be seen that the average values for the peak bending strains at IRJ2 show a higher variability compared with those for IRJ1 and the reference rail. For instance, with a 95% confidence level, ($\varepsilon/\varepsilon_y$) for IRJ2 is between 0.098 and 0.093, for IRJ1 it is between 0.127 and 0.124 and for the reference rail it is between 0.091 and 0.089.

One possible explanation for the higher variation in the data for IRJ2 under wheel passage is the higher frequency of the wheel passage over the sleepers adjacent to IRJ2. That is, less time is taken by a wheel to pass one sleeper spacing at the location of IRJ2 (due to the closely spaced arrangement of sleepers) compared with IRJ1. The sleeper spacing produces a periodic stiffness variation along the track which slightly excites the vehicle system. In this experiment a local change in sleeper spacing happens at the location of IRJ2. This might have caused some variability in the

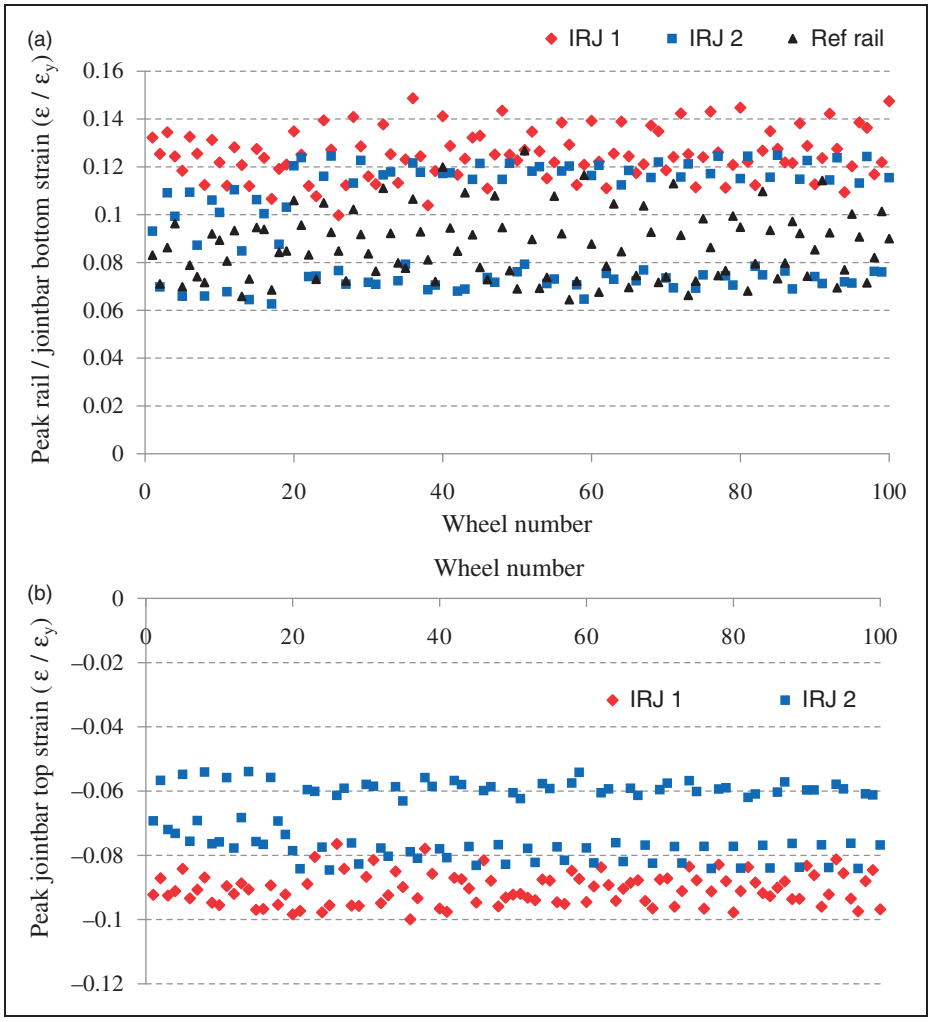

Figure 9. Peak bending strains extracted from the recorded data (a) rail foot and joint bar bottom and (b) joint bar top.

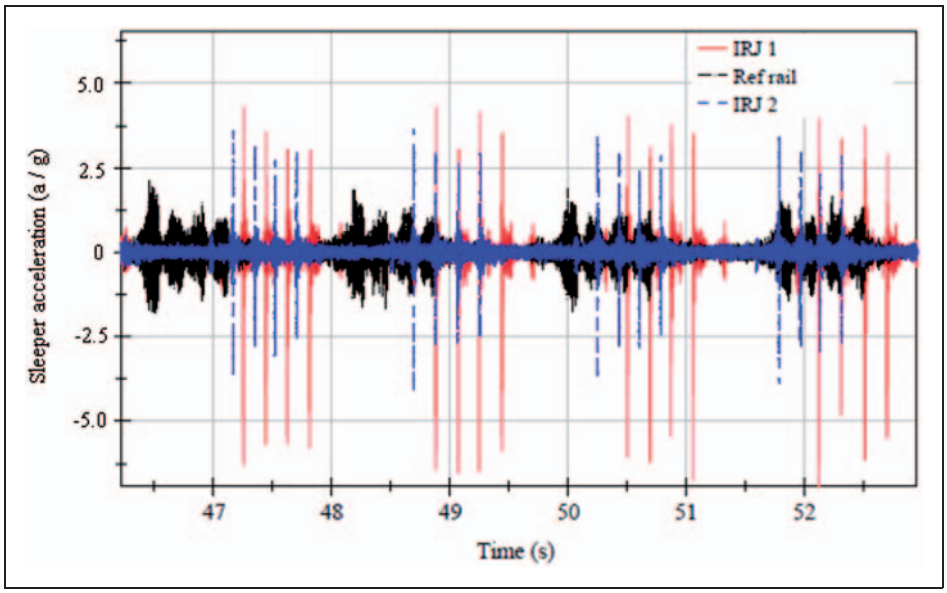

Figure 10. Time histories of sleeper acceleration for a 7 s train passage.

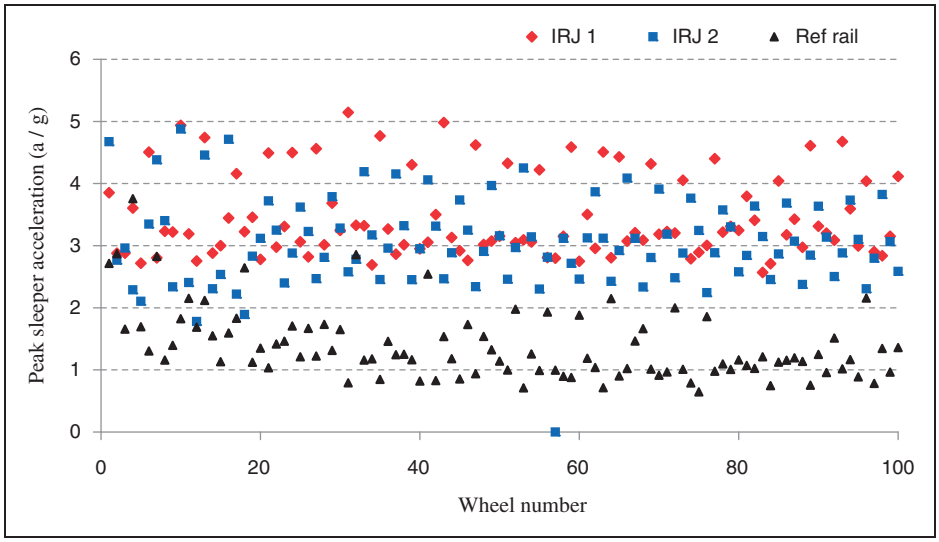

Figure 11. Peak acceleration values extracted from the data measured on the sleepers adjacent to IRJs and reference rail (running-on sleeper).

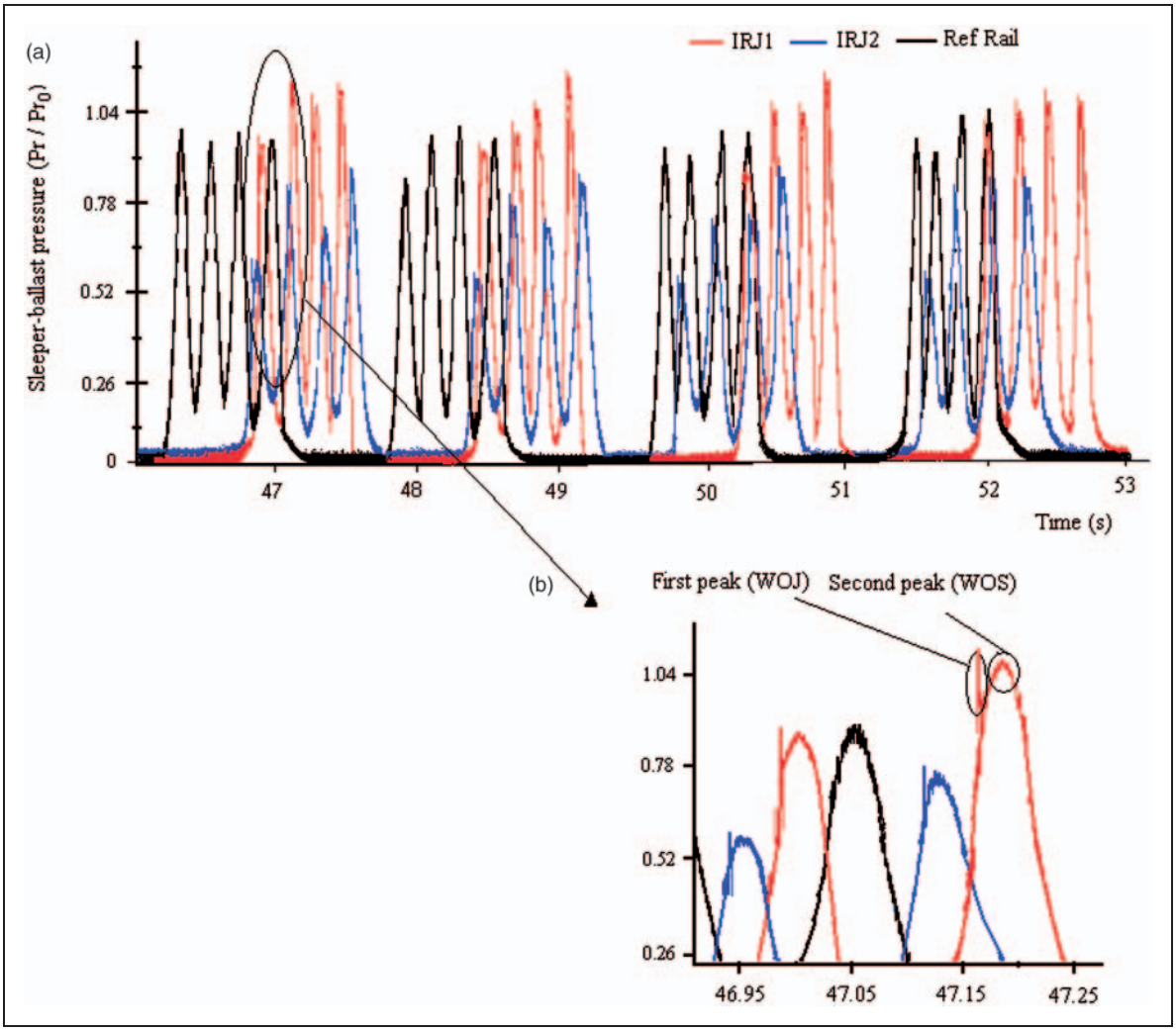

Figure 12. Time histories of sleeper–ballast pressure (a) a 7 s train passage and (b) an expanded view for 0.30 s.

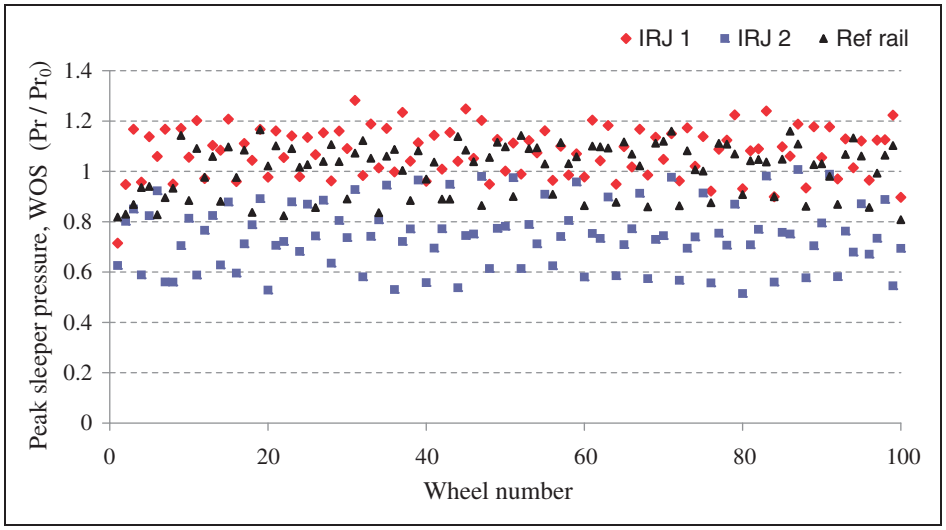

Figure 13. Peak pressure beneath the sleeper adjacent to IRJ: WOS.

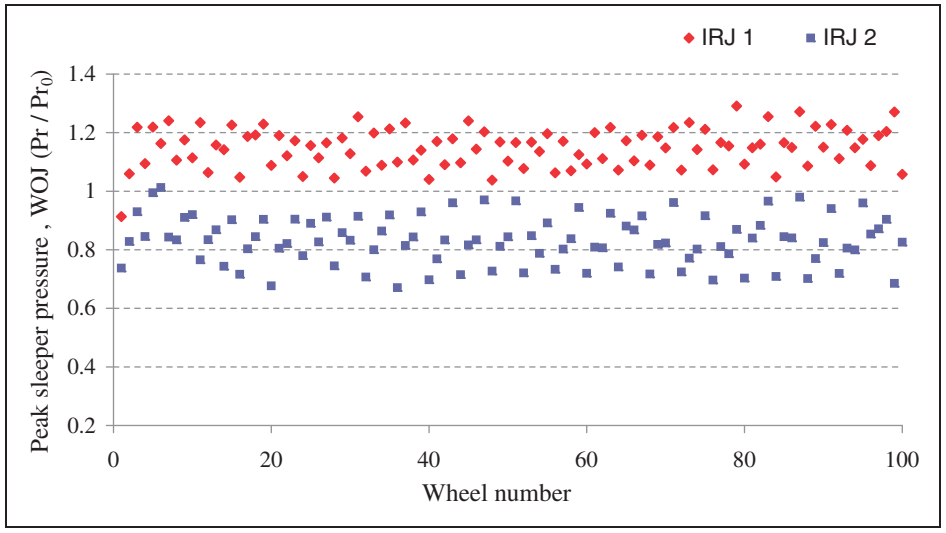

Figure 14. Peak pressure beneath the sleeper adjacent to IRJ: WOJ.

vehicle excitation resulting in a slightly higher variability in the responses at IRJ2 compared with those for IRJ1.

On average, the tensile strain at IRJ2 is about 28% lower than that at IRJ1; a result of the reduced span. Furthermore, the average values of the peak tensile bending strains at IRJ1 and IRJ2 are higher than that in the reference rail by about 40 and 8%, respectively. It should be noted that the sleeper spacing for IRJ2 is approximately half of that for the reference rail and the measured tensile strain location is closer to the neutral axis compared with that for the reference rail. Therefore, in the absence of the joint gap, the tensile strains in IRJ2 should have been much smaller than those in the reference rail. The 8% increase in the average peak tensile strains at IRJ2 should, therefore, be attributed to the higher peak (impact) load as well as the abrupt reduction of the stiffness compared with that of the reference rail. The 40% increase in the average tensile strain at IRJ1 relative to the reference rail (both have the same sleeper spacing) is also attributed to the impact load and reduced stiffness of the gapped section.

It can be seen in Figure 8 that the joint-bar top strain at IRJ2 shows higher positive values than at IRJ1. One physical explanation for this is that a larger negative bending moment is produced at the location of IRJ2 compared with that for IRJ1 when the wheel is away from the IRJs. However, please note that this does not affect the peak values presented in

Figure 9 as in this figure the values of the peak negative strains (compression strain) are presented and not the amplitude of the strain cycle.

Sleeper vertical acceleration

Figure 10 presents typical time histories of the vertical acceleration recorded at the sleepers adjacent to the gap of IRJ1 and IRJ2; the reference rail signature is also shown. The peaks correspond to the passage of the wheel over the concerned sleeper. Figure 11 presents a plot of the peak vertical acceleration corresponding to 100 passages of the wheels. In Figures 10 and 11, the acceleration data on the vertical axis are presented as the ratio of measured acceleration to the gravitational acceleration (a/g) where $g = 9.81\,\mathrm{m/s^2}$.

From Figure 11 it can be seen that the peak of the acceleration and the variability of both IRJs are much higher than for the reference rail. This indicates the effect of the presence of gaps in the IRJs compared with those for a continuous rail. The sleeper acceleration of IRJ2 is, on average, marginally lower than that of IRJ1, which can be attributed to the relatively higher number of sleepers attached to IRJ2, representing an increase in mass of the rail; an analogy is a forced vibrating string.

Sleeper–ballast pressure

The time histories of the sleeper–ballast pressures beneath the two IRJs and the reference rail for an approximately 7 s train passage is presented in Figure 12. It can be seen that the pattern of the sleeper–ballast pressure beneath the IRJs is different to that of the reference rail. The time histories of the pressure for the IRJs show two peak values for a single wheel passage. The first peak (short duration peak) happens when the wheel is over the joint gap and the second peak (long duration peak) happens when the wheel is over the sleeper. This confirms that a portion of the dynamic impact generated at the rail joint is transmitted to the track's substructure. This observation explains the high rate of track deterioration around the gap of the IRJs compared with that for continuous welded rails. This irregular sleeper–ballast pressure scenario beneath the sleepers around the IRJs is a key factor which gives rise to irregular track settlement and track geometry deterioration around the IRJs over a period of time. The deterioration of support beneath the IRJs can subsequently aggravate the loads and responses leading to overstressing and early failure of IRJ components. The peak values of the sleeper pressure were extracted from the recorded data and are compared in Figures 13 and 14. In Figures 12 to 14, the vertical axis represents the ratio of recorded ballast pressure (P_r) to the average value of ballast pressure recorded on the reference rail (P_{r0}). Figure 13 presents the peak values when the wheel is over the sleeper (WOS) and Figure 14 shows the peak values when the wheel is over the joint (WOJ). According to Figure 13, the average values of the peak sleeper pressure (long duration peak) at IRJ 2 is about 36% lower than that for IRJ1. According to Figure 14, the peak sleeper pressure (short duration peak) at IRJ2 is about 31% lower than that for IRJ1.

Conclusions

A field experiment involving two IRJs and a reference (continuous) rail has been presented. The wheel–rail vertical force, bending strains in rail/joint-bar, vertical acceleration of sleepers and the ballast pressure were measured. The following conclusions can be drawn from the presented work.

1. Shear bridged strain gauges can effectively measure the wheel loads.
2. Ballast beneath the sleeper adjacent to the joint gap is subjected to two peak loads under the passage of each wheel which means that the ballast beneath the IRJ can deteriorate at a higher rate compared with the average rate of track deterioration in a continuous rail section. It is possible to reduce the peak ballast pressure by closer positioning of the sleepers in the vicinity of the gaps of the IRJs.
3. The sleeper accelerations at the IRJs are higher than for the reference rail. This is due to the presence of dynamic loads as well as an abrupt reduction in the rail stiffness at the gap section compared with a continuous rail. The sleeper acceleration values at IRJ2 are lower than that at IRJ1. This is due to the relatively higher number of sleepers attached to IRJ2, causing an increase in track vibrating mass under the wheel.
4. Bending strains of the IRJs are significantly higher than the continuous rail due to an abrupt reduction in the rail stiffness at the gap section as well as the impact loading. The IRJ resting on closely spaced sleepers experienced lower bending compared with that for the IRJ with normally spaced sleepers but it is still higher than that experienced by the continuous rail.

The considerable difference in loads and track responses at locations in the vicinity of the gaps of the IRJs compared to continuous rails highlights the need for better guidelines and standards for installation and maintenance of IRJs in heavy haul tracks.

Funding

The Cooperative Research Centre for Rail Innovation Australia (Rail CRC), the Centre for Railway Engineering (CRE), Australian Rail Track Corporation (ARTC) and Queensland Rail (QR) supported the project financially and through in kind contributions. The research reported in this paper is part of R3.100 New Generation Insulated Rail Joint project.

Acknowledgements

The support of Robert Taylor and Ian Marks, the principal track engineers, and the help provided by Paul Boyd and Josh Mcdonald in installing the sensors and wayside DAQ system are gratefully acknowledged. Thermit Australia assisted in the manufacture of the strain gauged IRJs.

References

1. Kerr AD and Cox JE. Analysis and tests of bonded insulated rail joints subjected to vertical wheel loads. *Int J Mech Sci* 1999; 41: 1253–1272.
2. Plaut RH, Lohse-Busch H, Lambrecht S, et al. Analysis of tapered, adhesively bonded, insulated rail joints. *Proc IMechE, Part F: J Rail Rapid Transit* 2007; 221: 195–204.
3. Davis DD and Akhtar MN. Reduced impact bonded insulated joint designs. *Railw Track Struct* 2006; 102(8): 17–19.
4. Dhanasekar M and Bayissa W. Performance of square and inclined insulated rail joints based on field strain measurements. *Proc IMechE, Part F: J Rail Rapid Transit* 2012; 226(2): 140–154.
5. Suzuki T, Ishida M, Abe K and Koro K. Measurement on dynamic behaviour of track near rail joints and prediction of track settlement. *Q Rep RTRI* 2005; 46(2): 124–129.
6. Akhtar M, Davis D and Connor T. Revenue service evaluation of advanced design insulated joints, In: *The AREMA annual conference*, Salt Lake City, UT, 2008.
7. Kabo E, Nielsen JCO and Ekberg A. Prediction of dynamic train-track interaction and subsequent material deterioration in the presence of insulated rail joints. *Int J Veh Syst Dyn* 2006; 44: 718–729.
8. Wen Z, Jin X and Zhang W. Contact-impact stress analysis of rail joint region using the dynamic finite element method. *Wear* 2005; 258: 1301–1309.
9. Pang T and Dhanasekar M. Dynamic finite element analysis of the wheel-rail interaction adjacent to the insulated rail joints. In: *The seventh international conference on contact mechanics and wear of wheel/rail systems*, Brisbane, Australia: Institute of Materials Engineering, 2006, 509–516.
10. Askarinejad H, Dhanasekar M and Simson S. Effect of vertical misalignment of adjacent sleepers on the increase in dynamic loads around rail joints. In: *The conference on railway engineering*, Wellington, New Zealand, RTSA, 2010, pp.169–179.
11. Rail Infrastructure Corporation of New South Wales. *Specifications for supply of aggregates for ballast*, TS 3402, 2001. Sydney, Australia: Rail Infrastructure Corporation of New South Wales.
12. AS 1085.12:2002. Railway track material. Part 12: insulated joints assemblies.
13. Askarinejad H and Dhanasekar M. Determination of wheel-rail contact force at insulated rail joints. Research report on Project R3.100, Cooperative Research Centre for Rail Innovations, Australia, 2011.
14. Lee MK and Chiu WK. Determination of railway vertical wheel impact magnitudes; field trials. *Struct Health Monitor* 2007; 6(1): 49–65.
15. Johansson A and Nielsen JCO. Out-of-round railway wheels - wheel-rail contact forces and track response derived from field tests and numerical simulations. *Proc IMechE, Part F: J Rail Rapid Transit* 2003; 217: 135–146.
16. Dukkipati RV and Dong R. Impact loads due to wheel flats and shells. *Veh Syst Dyn* 1999; 31: 1–22.
17. Chebli H, Clouteau D and Schmitt L. Dynamic response of high-speed ballasted railway tracks: 3D periodic model and in situ measurements. *Soil Dyn Earthq Engng* 2008; 28: 118–131.
18. Indraratna B, Nimbalkar S, Christie D, et al. Field assessment of the performance of a ballasted rail track with and without geosynthetics. *J Geotech Geoenviron Engng* 2010; 136(7): 907–917.

Appendix 1

Notation

a	acceleration
g	gravitational acceleration
P	wheel–rail force
P_0	wheel–rail force at reference rail
P_r	Sleeper–ballast pressure
P_{r0}	sleeper–ballast pressure at reference rail
ε	strain
ε_y	rail steel yield strain